Landslide-triggering rainfall made more intense by human-induced climate change, devastating highly vulnerable communities in northern Kerala

Authors

1. Mariam Zachariah, *Grantham Institute - Climate Change and the Environment, Imperial College London, UK*
2. Chaithra S T, *Centre for Atmospheric Sciences, Indian Institute of Technology Delhi, India*
3. Dileepkumar R, *Department of Mathematics, KSMDB College Sasthamcotta, Kerala, India*
4. Arulalan T, *India Meteorological Department, Ministry of Earth Sciences, Gov. of India*
5. Clair Barnes*, Grantham Institute - Climate Change and the Environment, Imperial College London, UK*
6. Krishna AchutaRao, *Centre for Atmospheric Sciences, Indian Institute of Technology Delhi, India*
7. Arpita Mondal, *Civil Engineering Department, Indian Institute of Technology Bombay, India; IDP in Climate Studies, Indian Institute of Technology Bombay, India*
8. Manabendara Saharia, D*epartment of Civil Engineering, Indian Institute of Technology Delhi, India*
9. Maja Vahlberg, *Red Cross Red Crescent Climate Centre, The Hague, The Netherlands (based in Ubmeje/Umeå, Sweden)*
10. Friederike E L Otto, *Grantham Institute, Imperial College London, UK*

Review Authors

11. Joyce Kimutai, *Grantham Institute - Climate Change and the Environment, Imperial College London, UK*
12. Ben Clarke, *Grantham Institute - Climate Change and the Environment, Imperial College London, UK*
13. Sarah Kew, *Royal Netherlands Meteorological Institute (KNMI), De Bilt, The Netherlands*
14. Roop Singh, *Red Cross Red Crescent Climate Centre, The Hague, The Netherlands (based in New Jersey, USA)*
15. Sayanti Sengupta, *Red Cross Red Crescent Climate Centre, The Hague, The Netherlands (based in Berlin, Germany)*
16. Julie Arrighi, *Red Cross Red Crescent Climate Centre, The Hague, The Netherlands; Global Disaster Preparedness Centre, American Red Cross, Washington D.C., USA; University of Twente, Enschede, The Netherlands (based in New York, USA)*

17. Carolina Pereira Marghidan, *Red Cross Red Crescent Climate Centre, The Hague, The Netherlands; KNMI, De Bilt, the Netherlands; University of Twente, Enschede, The Netherlands (based in Utrecht, the Netherlands)*
18. Luis C. Rodriguez, *International Federation of Red Cross and Red Crescent Societies, Regional Office for Asia Pacific, Kuala Lumpur, Malaysia*

Main findings

- The Wayanad landslides resulted in devastating loss of life and occurred in a mountainous region with loose, erodible soils after 140mm of precipitation fell on saturated soils.
- In today's climate, which is 1.3°C warmer than it would have been at the beginning of the industrial period, an event of this magnitude is expected to occur about once every 50 years. The event is the third heaviest 1-day rainfall event on record, with heavier spells in 2019 and in 1924, and surpasses the very heavy rainfall in 2018 that affected large regions of Kerala.
- To assess if human-induced climate change influenced the heavy rainfall, we first determine if there is a trend in the observations. Heavy one-day rainfall events have become about 17% more intense in the last 45 years, over a period when the climate has warmed by 0.85°C. Longer-term trends in the pre-satellite era are not clear, which may relate to lower quality weather data.
- To quantify the role of human-induced climate change we analyse climate models with high enough resolution to capture precipitation over the relatively small study region. Overall, the available climate models indicate a 10% increase in intensity. Under a future warming scenario where the global temperature is 2°C higher than pre-industrial levels, climate models predict even heavier 1-day rainfall events, with a further expected increase of about 4% in rainfall intensity.
- Given the small mountainous region with complex rainfall-climate dynamics, there is a high level of uncertainty in the model results. However, the increase in heavy one-day rainfall events is in line with a large and growing body of scientific evidence on extreme rainfall in a warming world, including in India, and the physical understanding that a warmer atmosphere can hold more moisture, leading to heavier downpours.
- While the extreme rainfall was well forecast by the Indian Meteorological Department (IMD) and warnings were issued, the information was at the state-level, making it difficult to discern which localities would be impacted by landslides (one of the potential impacts of heavy rainfall listed in the warning) and would therefore require evacuation. Slope-specific landslide early warning systems can be extremely costly and difficult to implement, but those would provide the best opportunity for effective early action. Given this, reducing exposure of people and assets to landslide-prone places may be a more effective strategy.
- While the linkage between land cover and land use changes and landslide risk in Wayanad is mixed in the limited existing studies, factors such as quarrying for building materials, and a 62% reduction in forest cover, may have contributed to the increased susceptibility of the slopes to landslides when the heavy rain fell.
- The increase in climate change-driven rainfall found in this study is likely to increase the potential number of landslides that could be triggered in the future, raising the need for

adaptation actions that may include the reinforcement of susceptible slopes, landslide early warning systems, and construction of retaining structures to protect vulnerable localities.

1 Introduction

In the early hours of July 30, 2024, the villages of Mundakkai and Chooralmala in the district of Wayanad, Kerala experienced a catastrophic landslide, triggered by prolonged and intense rainfall. These villages are situated on the eastern slopes of the Vellarimala hills and a key tributary of the Chaliyar river flows near both villages. The initial landslide struck Mundakkai in the early morning hours, followed by three more landslides within a span of three hours, hitting areas like Chooralmala, Attamala, and Mundakkai. The event caused the collapse of the main bridge connecting the affected area to the nearest town, hindering rescue operations. The disaster resulted in over 400 fatalities, with hundreds more reported missing (ReliefWeb, 05 Aug 2024). The heavy rains caused the hillsides to give way, unleashing torrents of mud, water, and boulders that swept through the affected areas. The landslide began at an altitude of 1,550 metres, resulting in approximately 86,000 square metres of land being displaced (India Today). This landslide occurred less than 5 kilometres from a previous landslide site in 2019, which had resulted in 17 casualties (Desai, 2020).

Since June 22, the area has been subjected to nearly continuous rainfall, with only short breaks. Kalladi, situated 5 km from Mundakkai, has recorded around 1830 mm of rainfall over the past 30 days (IRDB), making it one of the wettest areas in Wayanad. On July 29, as Mundakkai in Wayanad received extremely heavy rainfall, the India Meteorological Department (IMD) issued an 'orange alert' for the district. Over 12 hours later, the first landslide occurred (The Hindu, 02 Aug 2024; The News Minute, 31 July 2024). The continuous precipitation, combined with dense cloud cover, low-level wind convergence, and orographic effects, likely triggered landslides on the nearby slopes, leading to the disaster by midnight on July 30. By July 30, the IMD upgraded the alert to red, with a warning of “extremely heavy rain” but the landslides had already caused massive destruction, with over 400 deaths and 152 missing (The Times of India, 07 August 2024). A rain gauge located in nearby Puthumala, maintained by Hume Centre for Ecology and Wildlife Biology, recorded 572 mm of rainfall in the 48 hours leading to the landslides (The New Indian Express, 31 July 2024; Mathrubhumi, 2024). Experts noted the need for monitoring rainfall in landslide hotspots; the IMD’s rain gauge in Vythiri recorded significantly lower rainfall than the measured in the impacted regions (The Wire, 2024) .

For two weeks prior to the event, the districts of Kasargod, Kannur, Wayanad, Calicut, and Malappuram experienced heavy rainfall due to an active monsoon offshore trough affecting the entire Konkan region, leading to saturated soils in these parts (India Today; The Economic TImes). Following this period, a deep mesoscale cloud system developed off the Arabian Sea on Monday, leading to extremely heavy precipitation in North Kerala- over the districts of Wayanad, Calicut, Malappuram, and Kannur, reportedly triggering the landslides (India Today; The Economic TImes). Similar synoptic scale systems were present during extreme rainfall events that led to the catastrophic floods in Kerala in 2018 (Hunt and Menon, 2020; Kumar et al.,2020; Suneela et al., 2023; Dhasmana et al., 2023).

Previous studies that have explored the relationship between omega (vertical velocity in pressure coordinates) and extreme precipitation events (Nie et al. 2016; Pauley and Nieman 1992; Nie and Fan

2019; Agel et al. 2019) identify topographically forced ascent as the most critical dynamical factor. The vertical velocity (omega) profile over North Kerala, averaged between 75°E and 77°E longitude for the 29th of July over Wayanad over 900 to 850 hPa, shows strong negative values (Figure 1) indicating extreme rainfall over the Wayanad region (11.4°N and 12°N). The vertical velocity profile on 30th July also shows negative values over 900 to 850 hPa, however, the values are positive between 750 and 500 hPa levels, following the landslides that occurred in the earlier hours of the day. Vertically integrated moisture flux (VIMF) is determined by vertically integrating (1000 to 100 hPa) the moisture fluxes of the u and v wind components. The dynamic aspect of VIMF, driven by wind, plays a significant role in regions affected by landfalling atmospheric rivers, tropical cyclones, or moisture-transporting low-level jets (Gimeno et al., 2023). Consequently, extreme precipitation events are closely associated with atmospheric moisture transport (Raghuvanshi and Agarwal, 2023). On July 29th and 30th, a strong moisture flux was observed over the northern Kerala region, with all atmospheric circulation patterns favouring an extreme rainfall event in the Wayanad district.

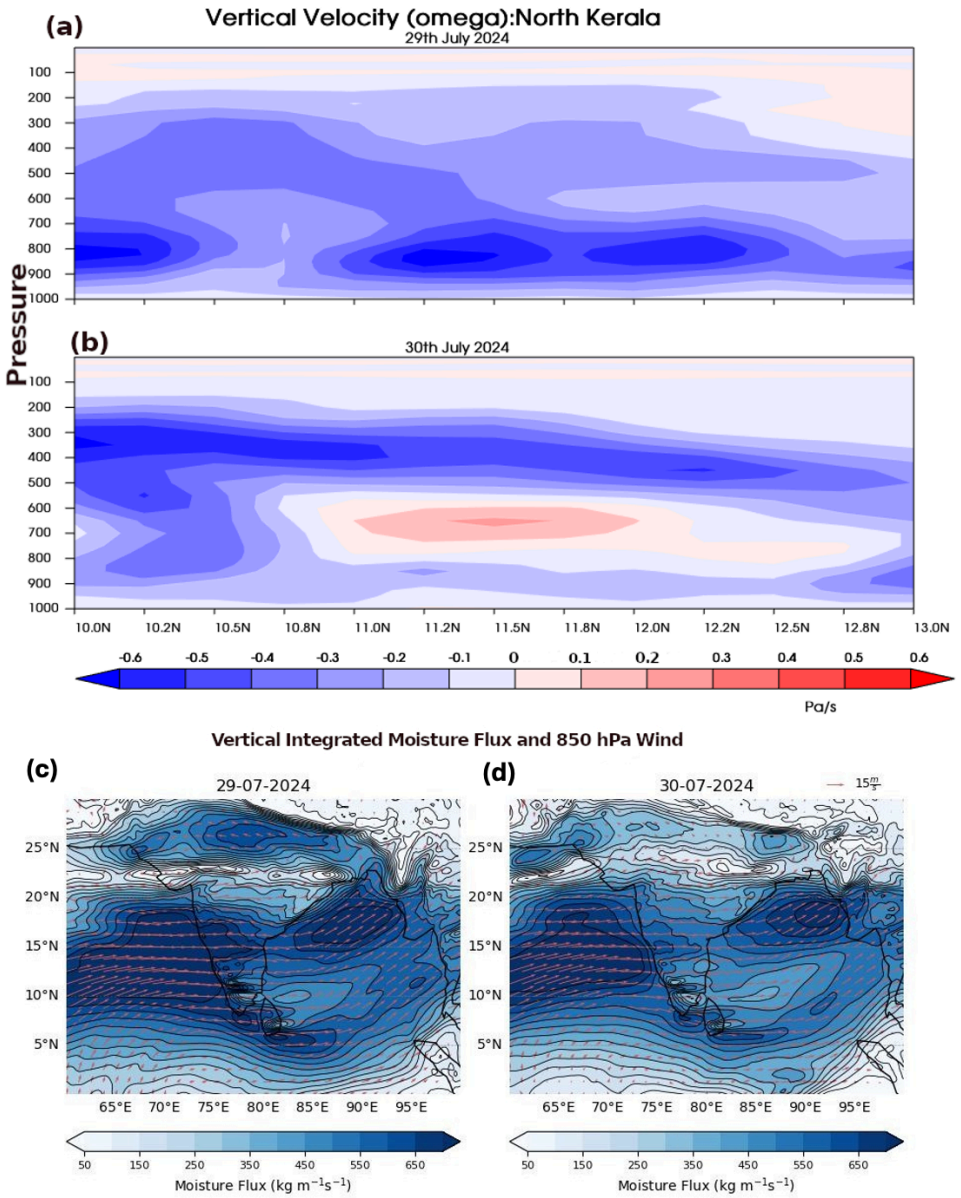

Figure 1: *(a-b) Vertical velocity (omega) profile over North Kerala, averaged between 75°E and 77°E longitude for (a) July 29th and (b) July 30th, 2024, based on ERA5 Reanalysis data. Negative values indicate strong upward air movement. The landslide-affected district of Wayanad is situated between 11.4°N and 12°N latitude. (c-d) Vertically integrated moisture flux (1000 to 100 hPa; shading) for (c) July 29th and (d) July 30th 2024, overlaid with 850 hPa wind vectors (arrows), based on ERA5 reanalysis data.*

1.1 Event definition

The hilly regions of Wayanad are particularly prone to landslides due to a combination of factors including steep slopes, high elevation, prolonged rainfall, and significant land-use changes (Arumugam et al., 2023). These conditions contribute to landslides being a recurrent and severe issue in the area. This year, the rainfall from the synoptic systems that reportedly triggered the landslides fell over much of northern Kerala, including the districts of Malappuram, Kannur and Kozhikode in the north, and also reaching Cochin to the south.

Figure 2 shows the rainfall on 30 July 2024 in the IMD dataset (aggregated from 0830 29 July 2024 IST to 0830 30 July 2024 IST). The study region (highlighted in red) encompasses all of Kerala above 10N. The area-averaged daily rainfall time series for the study region identifies this event as the highest rainfall yet recorded in the ongoing 2024 JJAS season. Consequently, for the purpose of our attribution study, we define this event as the 1-day maximum of the daily rainfall averaged over the study region during the monsoon season (JJAS), hereafter referred to as JJAS Rx1day.

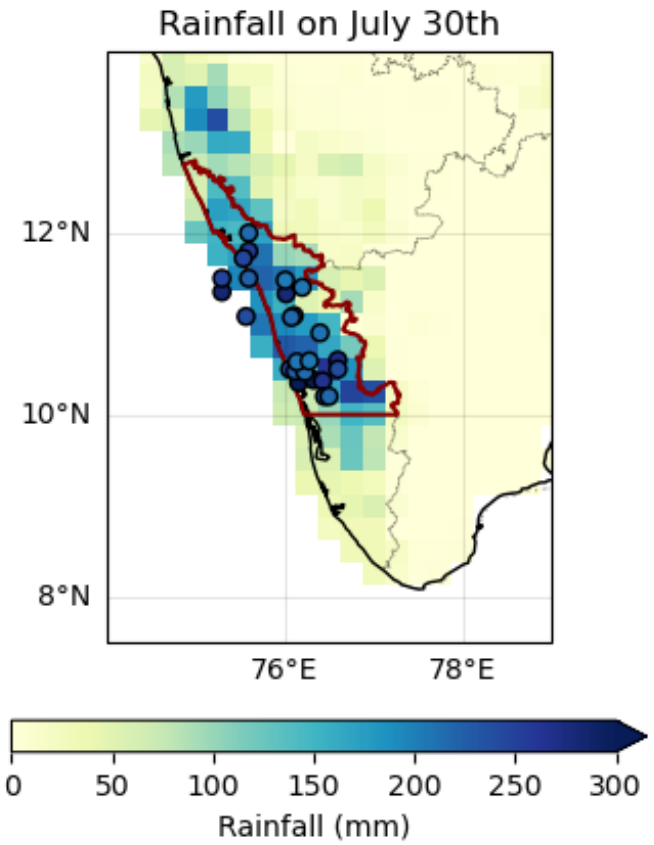

Figure 2: *Rainfall on the 30th of August, 2024 in IMD. The red highlight indicates the study region.The scatter shows the rainfall on the day recorded over IMD stations in the study region on the day.*

1.2 Literature on changes in extreme rainfall in the region

Studies have shown a global increase in extreme precipitation events due to global warming, with significant regional variability observed in Europe, Asia, Africa, and America (Alexander et al., 2006; Zhang et al., 2013; Donat et al., 2016). Although regional variability exists, particularly global trends indicate a likely rise in both the frequency and intensity of heavy precipitation, with projections showing further increases by the end of the century (Alexander et al., 2017; Seneviratne et al., 2021). In line with these global observations, studies have reported a similar increase in extreme precipitation events across various regions in India (Rajeevan et al., 2008; Krishnamurthy et al., 2009; Pai and Sridhar 2015). Notably, changes in extreme precipitation have been particularly evident over central India since the 1950s (Roxy et al., 2017; Malik et al., 2016). A rise in the annual maximum rainfall from 1951-2015 across India was observed by Mukherjee et al. (2018). They found that this increase was more pronounced in southern India, particularly after 1982. Suman and Maity (2020) found that extreme precipitation during the Indian Summer Monsoon has intensified more significantly in southern India than in northern and central India between 1971 and 2017, using 1930-1970 as the reference period. A study by Boyaj et al. (2020) analyses land use and land cover (LULC) data from 2005 and 2017, revealing significant changes in Tamil Nadu, Telangana, and Kerala, primarily due to urbanisation and changes in forest types - especially the change of the dominant mixed forest type in Kerala into deciduous needle/leaf forests. Sensitivity experiments using the WRF model show that

these LULC changes, particularly increased urbanisation, lead to higher surface temperatures, increased heat fluxes, and more intense rainfall.

Regional precipitation extremes in India are strongly influenced by the Indian Summer Monsoon (ISM) circulation. The southwest monsoon, which occurs from June to September and accounts for 70-90% of the annual rainfall is driven by thermal lows over northwest India due to the temperature contrast between land and the Indian Ocean. Orographic effects, such as the influence of mountain ranges like the Western Ghats and the eastern Himalayas, significantly shape the spatial distribution of rainfall, with the heaviest rainfall typically occurring in these mountainous regions and along the west coast, the Himalayan foothills, and northeast India. The ISM is driven by factors such as the monsoon trough, offshore troughs along the west coast, and the movement of monsoon lows and depressions (Rao, 1976). The steep topography of the Western Ghats interacts with moist ISM winds to generate deep convective systems, resulting in daily rainfall ranging from 10 to 100 mm (Guhathakurta et al., 2015). Additionally, offshore troughs along the west coast and depressions forming over the Bay of Bengal, which move toward central India, enhance moisture convergence and lead to heavy rainfall (Francis and Gadgil, 2006). A study by Sandeep and Ajayamohan (2015) found that the low-level jetstream (LLJ), which is crucial for transporting moisture to India and driving the Indian summer monsoon, are shifting polewards in response to global warming. This shift, observed in both observations and climate models, has led to drying in the southern and wetting in the northern parts of India's western coast over the past three decades. The poleward shift of the LLJ and changes in moisture distribution are associated with increased land-sea contrasts and a stronger pressure gradient over the Indian Ocean. Future projections suggest that this shift will persist, with varying impacts based on the level of global warming. They also indicate that these changes are especially significant for the ecologically sensitive areas in Western Ghats.

The west coast of India frequently experiences regional flooding during the monsoon season due to extreme rainfall, primarily driven by the interaction of low-level monsoon winds with the Western Ghats, coupled with the development of synoptic-scale convective systems. Jamshadali et al. (2021) analysed 65 years of data from 1951 to 2015 and found that the west coast of India is highly prone to extreme rainfall events during the summer monsoon. These heavy rains are largely driven by synoptic systems such as offshore troughs and vortices, linked to atmospheric conditions over the equatorial Indian Ocean (Francis and Gadgil, 2006). However, studies also show a notable weakening of both mean rainfall and vertical velocities during the monsoon season in the orographic regions of the Western Ghats (Rajendran et al., 2012). Recent trends indicate that extreme rainfall events have increased along the west coast of India, particularly in regions such as Konkan & Goa, while the frequency of lighter and moderate rainfall has decreased, reflecting a shift towards more intense and inconsistent rainfall patterns (Prathipati et al., 2019). Additionally, a recent study showed that rainfall along the west coast of India is shifting towards more convective patterns, with deeper, ice-rich clouds and increased convection intensity (Sreenath et al., 2022). Sreenath et al. (2023) show that extreme rainfall events are becoming more common along the southwest coast of India, in which the frequency of extreme rainfall has decreased between 14° and 16°N along the northwest coast, while the southwest coast has become a hotspot for such events. They link this shift to the increased sea surface temperature(SST) gradient between the north and south Arabian Sea, driven by the warming of the south-central Arabian Sea, and to low-pressure systems over the Bay of Bengal prior to the occurrence of extreme rainfall. The study suggests that these factors facilitate the shift of moisture-laden winds from the northwest to the southwest coast. The reviewed literature on rainfall trends across different

aggregation-scales highlights how global warming's thermodynamic effects can intensify rainfall extremes, even while dynamic processes, such as the poleward shift of the monsoon discussed above, can lead to long-term drying trends by affecting mean seasonal precipitation trends.

1.3 Past extreme rainfall events in Kerala: the 1924 and 2018 deluges

Kerala, located in the southwestern part of the Indian peninsula, situated in the southern Western Ghats, experiences around 2,000 mm of seasonal rainfall with unique rainfall patterns due to the orographical features of western ghats. The first flood officially recorded in Kerala happened in 1881 (KSDMA, 2018). In July 1924, Kerala was struck by the devastating Great Flood of 1924. This catastrophic event was triggered by severe flooding of rivers originating from the Sahyadri Mountains, with intense rainfall lasting nearly three weeks and inundating many districts across the state. The flood caused a tragic loss of thousands of lives, both human and animal, and inflicted widespread damage to infrastructure, including buildings, roads, and crops. Following the catastrophic floods of 1924, Kerala faced the next severe flood event in August 2018, considered the most devastating since 1924. This flood was triggered by exceptionally heavy rainfall, leading to intense flooding and severe landslides isolating the hilly districts of Wayanad and Idukki (KSDMA 2018). This once in a 100 year-flood, often referred to as the 'Flood of the Century,' caused 500 casualties and $5 billion in damage (CWC report, 2018; Hunt and Menon, 2020). With 35 out of 54 dams being opened for the first time in history, exacerbated the flooding, causing extensive damage to crops and livestock. The impact was widespread, affecting the entire state of Kerala with several days of heavy rainfall. According to the India Meteorological Department (IMD), the rainfall in August 2018 was the highest recorded in Kerala in the past 78 years (Yesubabu, et al., 2019). A probabilistic extreme event attribution analysis on the 2018 Kerala floods found that the event could not be attributed to human-induced climate change (Dhasmana et al., 2023), both in terms of heavy rainfall and high river flows.

2 Data and methods

2.1 Observational data

Four gridded datasets were considered in this study for analysing rainfall extremes in the region:

1. *IMD station-based observed rainfall* which includes data from synoptic observations, and Automatic Weather Systems maintained and observed by India Meteorological Department (IMD), at 3-hourly and hourly intervals, respectively. Some of these stations are maintained and observed by the State authorities; these stations form a major input to the preparation of IMD gridded rainfall dataset. These data are available upon request from the data supply portal of IMD. In this study, May-Aug 2024 stations-based IMD observed rainfall over Kerala state has been used for validation of IMD gridded dataset.
2. *IMD gridded rainfall* dataset developed and maintained by IMD, at daily timesteps beginning in the year 1901 and available till 2024-Aug-02, at the time of this study. The gridded rainfall dataset is developed using the inverse distance weighting method based on records from a variable network of rain gauge stations across India (6955 rain gauge stations with varying availability periods- Pai et al., 2013).

3. *CPC gridded rainfall* from Climate Prediction Centre (CPC), a product from NOAA PSL, Boulder, Colorado, USA and known as the CPC Global Unified Daily Gridded data. This is available from NOAA at 0.5° spatial resolution covering the period 1979-present.
4. MSWEP gridded rainfall dataset, or the Multi-Source Weighted-Ensemble Precipitation (MSWEP) dataset (updated from Beck et al., 2019) is a product that combines gauge-, satellite-, and reanalysis-based data for reliable precipitation estimates, at daily intervals from 1979 to near real-time, and at 0.1° spatial resolution globally.
5. *ERA5 Reanalysis v5 gridded rainfall* from the European Centre for Medium-Range Weather Forecasts (ECMWF) which starts in the year 1940 (Hersbach et al., 2020), and available at 0.25° spatial resolution. It should be noted that the variables from ERA5 are not directly assimilated, but these are generated by atmospheric components of the Integrated Forecast System (IFS) modelling system. Daily rainfall data from this product starting from the year 1950, available at 0.5° × 0.5° from the Climate Explorer was utilised for this study. At the time, the re-analysis was available until the end of June 2024. This was extended with the ECMWF analysis (1-28 June) and the ECMWF forecast (29 July -2 August) to cover the days including the day of the event.

Finally, as a measure of anthropogenic climate change we use the (low-pass filtered) global mean surface temperature (GMST), where GMST is taken from the National Aeronautics and Space Administration (NASA) Goddard Institute for Space Science (GISS) surface temperature analysis (GISTEMP, Hansen et al., 2010 and Lenssen et al. 2019).

2.1.1 Evaluation of the selected observed datasets for the study

By considering the gauge-based interpolated IMD gridded dataset as the reference data, we first evaluated the other three gridded rainfall datasets- CPC, MSWEP and ERA5 for their fidelity in terms of their ability to capture the event under study and the long-term trends and the year-to-year variability.
Figure S1 shows the rainfall over the study region on the days around the landslides in Wayanad, for the four datasets. Albeit the small differences arising from the grid resolution, the CPC, ERA5 and MSWEP are all found to be generally reliable in terms of capturing the spatial rainfall distribution with the heaviest rainfall on the local day of the landslide- 30-07-2024 in IMD which is aggregated following Indian Standard Time (IST) and on 29-07-2024 in the global gridded datasets that are aggregated at Coordinated Universal Time (UTC).

Figure S2 shows the daily rainfall distribution in each dataset, area-averaged over the study region, for all available years up to 31st July 2024. The daily rainfall in the global datasets are found to be consistent with IMD, to varying extents. CPC and ERA5 datasets are found to be good in capturing the heavier monsoon (June-September) and the milder winter (October-Dec) peaks in the IMD data. These peaks are not as distinct in MSWEP, with some years in the past showing unusually high rainfall even in the drier spring months of February and March. The rainfall distribution for this year (black line in Figure S2) in CPC is consistent with IMD, both in day-to-day variability and in capturing the extremity of the 1-day rainfall on the 30th of July that triggered the landslides, while the event is not extreme in the other two datasets. The ERA5 dataset also shows three days of unusually high rainfall in mid -May over North Kerala, (which is also the highest rainfall in this year, according

to this dataset) that is not seen in IMD. Finally, upon evaluating the long-term trend and the year-to-year variability in one-day extreme rainfall during JJAS in these datasets, both ERA5 and MSWEP datasets were found to underestimate the rainfall during the event by at least 60 mm, and was not the heaviest spell in the season as was the case in IMD (Fig. S3). The CPC dataset on the other hand was able to mirror this extreme nature of the 2024 event but with an underestimated magnitude likely an artefact of this dataset's coarser resolution as compared to IMD. For these reasons, the IMD and CPC datasets are used as the primary observed data for the rest of the study, and the other two datasets are excluded.

It has been observed in past studies comparing the IMD gridded product with other satellite-based products that the interpolation algorithm used for the creation of the IMD dataset may have introduced a positive bias in rainfall trends after the year 1975 (Lin and Huybers, 2018; Goteti and Famiglietti, 2024). This has been ascribed to the sudden increase in the number of observing gauges during the 1970s (see Fig. 2 in Pai et al. (2014) for the daily variation in the number of observing rain gauges that go into the creation of the IMD product). Lin and Huybers (2018) further showed that it is the trends evaluated across this jump that is suspect. Following from this, we include the IMD dataset for two time slices- (1) a long-term period (1901-2024), which includes the 1970s, and (2) a short-term period (1979-2024), which occurs after the suspect period and aligns better with satellite-based estimates. This is done to help provide a more reliable assessment of rainfall trends and reduce the potential bias introduced by the changes in gauge density and satellite-based product during the 1970s. An additional aspect that remains unexplored in this study is the potential influence of aerosols, such as black carbon from crop-burning—known to affect rainfall and temperature patterns in northern India—and dust carried in from neighbouring arid regions, on long-term trends in local and regional rainfall in the study region and surrounding area. While some research, including studies by Lau and Kim (2006), Ramachandran and Kedia (2013), Kumar and Manjunatha (2021), and Jasmine et al. (2022), have highlighted these factors using observational data and climate models, the current body of work is insufficient to draw definitive conclusions about the sensitivity of these trends to the length of the data record as reported above. Further investigation is required to fully understand the impact of aerosols on rainfall trends and their broader climatic implications.

2.2 Model and experiment descriptions

We use 3 multi-model ensembles from climate modelling experiments using very different framings (Philip et al., 2020): Sea Surface temperature (SST) driven global circulation high resolution models, coupled global circulation models and regional climate models.

1. Coordinated Regional Climate Downscaling Experiment CORDEX-CORE over the West-Asia domain with 0.22 km resolution (WAS-22) (Teichman et al., 2021). The ensemble consists of 3 regional climate models downscaling 6 GCMs. These simulations are composed of historical simulations up to 2005, and extended to the year 2100 using the RCP8.5 scenario.

2. CMIP6. This consists of simulations from 9 participating models with varying resolutions. For more details on CMIP6, please see Eyring et al., (2016). For all simulations, the period 1850 to 2014 is based on historical simulations, while the SSP2-4.5 scenario (2015-2100) is used for the remainder of the 21st century. The daily precipitation data from the models was interpolated to a uniform spatial

resolution of 1°×1° before performing the model evaluation. The regridding method employed was bilinear regridding.

3. HighResMIP SST-forced model ensemble (Haarsma et al. 2016), the simulations for which span from 1950 to 2050. In this study, 4 models from this experiment were evaluated. The SST and sea ice forcings for the period 1950-2014 are obtained from the 0.25° x 0.25° Hadley Centre Global Sea Ice and Sea Surface Temperature dataset that have undergone area-weighted regridding to match the climate model resolution. For the 'future' time period (2015-2050), SST/sea-ice data are derived from RCP8.5 (CMIP5) data, and combined with greenhouse gas forcings from SSP5-8.5 (CMIP6) simulations (see Section 3.3 of Haarsma et al. 2016 for further details).

2.3 Statistical methods

In this analysis we examine time series of JJAS RX1day values over the study region, where long records of observed data are available. Methods for observational and model analysis and for model evaluation and synthesis are used according to the World Weather Attribution Protocol, described in Philip et al. (2020), with supporting details found in van Oldenborgh et al. (2021), Ciavarella et al. (2021) and here.

The analysis steps include: (i) trend calculation from observations; (ii) model validation; (iii) multi-method multi-model attribution and (iv) synthesis of the attribution statement.
We calculate the return periods, Probability Ratio (PR; the factor-change in the event's probability) and change in intensity of the event under study in order to compare the climate of now and the climate of the past, defined respectively by the GMST values of now and of the preindustrial past (1850-1900, based on the Global Warming Index). To statistically model the event under study, we use a GEV distribution that scales with GMST. Next, results from observations and models that pass the validation tests are synthesised into a single attribution statement.

3 Observational analysis: return period and trend

23.1 Analysis of gridded data

The left panels in Figure 3 show the response of JJAS maximum 1-day rainfall area-averaged over the study region to the global mean temperature, based on the IMD and CPC datasets for the period 1979-2024. There is an increasing trend in the intensity of Rx1day in both datasets in response to global warming. The right panels in Figure 3 shows the return period curves, for the 2024 climate and a 1.3 °C cooler climate. The 2024 event has a return period of 22 years (uncertainty: 4 - 1.5E+07 years) in the IMD dataset; in CPC, the event has a return period of 12 years (uncertainty: 5 - 70 years). The probability ratio between the present 2024 climate vs. 1.3 °C cooler climate suggests a strong increase in the likelihood (albeit with uncertainty encompassing no change) of an event such as this in both datasets, with a best estimated PR of 6.87 (uncertainty: 0.112 to 1.5E+07) for IMD and 3.25 (uncertainty: 0.38 to 178.5) for CPC. These increases in likelihood are associated with intensity increases of 30.98% (uncertainty: 25.95% decrease to 174.12% increase) and 27.86% (16.45% decrease to 99.14% increase) in the IMD and CPC datasets, respectively. Given that almost 0.85degC of the 1.3degC warming since pre-industrial climate happened since 1980, we also estimate these

changes for the satellite-era (1979-2024). Heavy one-day rainfall events have become about 19% more intense (uncertainty: 17.1% decrease to 81.5% increase) and 3.22 times more likely(uncertainty: 0.2 to inf) in the last 45 years, in IMD, and 17.4% more intense (uncertainty: -11.4 % decrease to 55% increase) and 2.13 times more likely (uncertainty: 0.51 -26.7) in CPC.

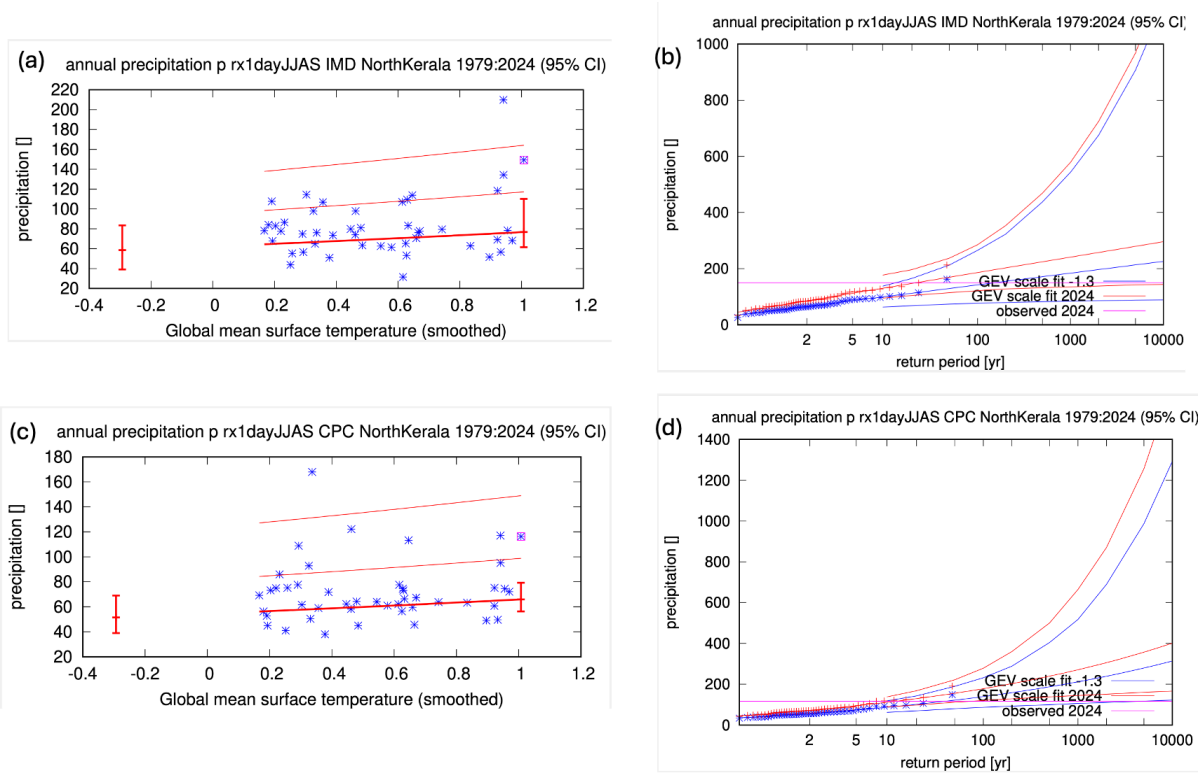

Figure 3: *GEV fit with constant dispersion parameters, and location parameter scaling proportional to GMST of the index series, for the Indus river basin based on three gridded datasets- (a) IMD (b) and (b) CPC, for the period 1979-2024. The 2024 event is included in the fit.* ***Left****: Observed max.1-day average rainfall in the JJAS season as a function of the smoothed GMST. The thick red line denotes the time-varying location parameter. The vertical red lines show the 95% confidence interval for the location parameter, for the current, 2024 climate and a 1.3ºC cooler climate. The 2024 observation is highlighted with the magenta box.* ***Right****: Return time plots for the climate of 2024 (red) and a climate with GMST 1.3 ºC cooler (blue). The past observations are shown twice: once shifted up to the current climate and once shifted down to the climate of the late nineteenth century. The markers show the data and the lines show the fits and uncertainty from the bootstrap. The magenta line shows the magnitude of the 2024 event analysed here.*

As discussed in Section 2.1.1, we also analyse the trends in the long-term IMD dataset separately. Figure 4 shows the results for the IMD dataset-based time series upon including the entire length of data from 1901-2024. This longer time series shows slightly declining trends in response to increasing GMST. The 2024 event is slightly more extreme in this series, with a higher return period of 71 years (uncertainty: 21-250 years) with the 2024 event made less likely by climate change with PR of 0.576 (uncertainty: 0.067 to 7.797) and made less intense with a best estimate of 7.387% decrease (uncertainty: 25% decrease to 16.063% increase).

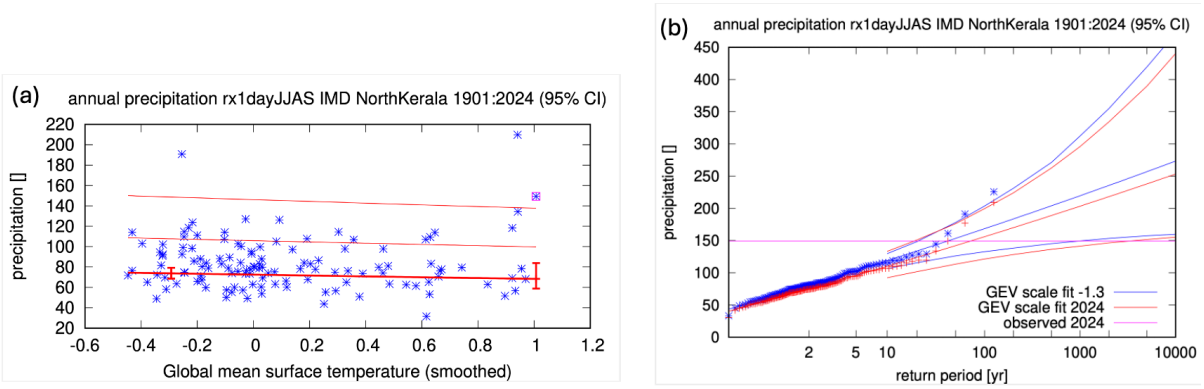

Figure 4: *as Figure 3, for IMD dataset, considering years from 1901-2024.*

Over the 46 years from 1979 to 2024, the 2024 rainfall event has only been surpassed once in the IMD dataset, during the year 2019, and twice in the CPC dataset, during 2019 and 1991. However, the 1991 event in the CPC dataset is likely an artefact of its coarser resolution and does not appear in any of the other datasets (see Fig. S2). In the long-term IMD series, the highest one-day extreme rainfall was recorded in 1924, associated with the Great Flood of '99, followed by the 2019 event. Thus, for the purpose of attribution assessment, we define the 2024 event as a 1-in-50-year event, based on a rounded average of the best estimated return periods from both the short-term and long-term IMD time series, making it a reasonable estimate.

4 Model evaluation

In this section we show the results of the model evaluation for the assessed region. The climate models are evaluated against the observations in their ability to capture:

1. Seasonal cycles: For this, we qualitatively compare the seasonal cycles based on model outputs against observations-based cycles. We discard the models that exhibit ill-defined peaks in their seasonal cycles. We also discard the model if the rainy season onset/termination varies significantly from the observations.

2. Spatial patterns: Models that do not match the observations in terms of the large-scale precipitation patterns are excluded.

3. Parameters of the fitted GEV models. We discard the model if the model and observation parameters ranges do not overlap.

The models are labelled as 'good','reasonable', or 'bad' based on their performances in terms of the three criteria discussed above. A model is given an overall rating of 'good' if it is rated 'good' for all three characteristics. If there is at least one 'reasonable', then its overall rating will be 'reasonable' and 'bad' if there is at least one 'bad'.

Per framing or model setup we also use models that only just pass the validation tests if we only have five models or less for that framing that perform well. The tables show the model validation results. Table 1 shows the model evaluation results for this study region. We note that out of the 25 models from the three modelling experiments (CORDEX, HighResMIP and CMIP6) used in the model-based

evaluation and attribution, only two were evaluated ‘good’ (both from the seven participating models from the HighResMIP experiment) . Four out of the nine models under CORDEX, three models from HighResMIP and seven out of the nine models under CMIP6 were classified as ‘reasonable’, and the remaining as ‘bad’. Therefore, we select the 16 models that qualify as ‘reasonable’ to ‘good’ for the attribution analysis.

***Table 1**: Evaluation results of the climate models considered for attribution analysis of Rx1day over the study region. For each model, the best estimate of the dispersion and the 95% confidence interval obtained via bootstrapping. The rows are highlighted in green, yellow and red for highlighting the models that were ranked as ‘good’, ‘reasonable’ and ‘bad’, respectively.*

Model / Observations	**Seasonal cycle**	**Spatial pattern**	**Sigma**	**Shape parameter**	**Event magnitude (mm)**
IMD (1979-2024)			0.310 (0.209 ... 0.380)	0.0 (-0.48 ... 0.34)	
CPC			0.257 (0.192 ... 0.302)	0.15 (-0.092 ... 0.38)	
IMD (1901-2024)			0.265 (0.219 ... 0.304)	-0.022 (-0.18 ... 0.17)	
CORDEX					Threshold for 50-year event (mm)
EC-EARTH_rcp85_r12i1p1_ETH-COSMO-crCLIM-v1-1 CORDEX (1)	bad	good	0.217 (0.156 ... 0.255)	-0.012 (-0.36 ... 0.59)	262.98
HadGEM2-ES_rcp85_r1i1p1_REMO2015 CORDEX (1)	bad	bad	0.163 (0.106 ... 0.201)	-0.11 (-0.57 ... 0.19)	317.85
MIROC5_rcp85_r1i1p1_RegCM4-7 CORDEX (1)	good	reasonable	0.372 (0.242 ... 0.455)	0.37 (0.12 ... 0.87)	267.29
MPI-ESM-LR_rcp85_r1i1p1_ETH-COSMO-crCLIM-v1-1 CORDEX (1)	reasonable	good	0.297 (0.199 ... 0.361)	0.34 (-0.033 ... 0.95)	367.43
MPI-ESM-LR_rcp85_r1i1p1_REMO2015 CORDEX (1)	good	bad	0.248 (0.167 ... 0.306)	-0.22 (-0.66 ... 0.065)	230.76
MPI-ESM-MR_rcp85_r1i1p1_RegCM4-7 CORDEX (1)	reasonable	reasonable	0.395 (0.257 ... 0.465)	0.34 (-0.040 ... 1.1)	167.76
NorESM1-M_rcp85_r1i1p1_ETH-COSMO-crCLIM-v1-1 CORDEX (1)	reasonable	good	0.361 (0.252 ... 0.438)	-0.0082 (-0.47 ... 0.38)	323.58
NorESM1-M_rcp85_r1i1p1_RegCM4-7 CORDEX (1)	bad	bad	0.332 (0.207 ... 0.403)	0.12 (-0.13 ... 0.51)	111.32
NorESM1-M_rcp85_r1i1p1_REMO2015 CORDEX (1)	good	bad	0.328 (0.230 ... 0.393)	-0.23 (-0.61 ... 0.11)	234.61
HighResMIP					
FGOALS-f3-L HighResMIP (1)	reasonable	reasonable	0.242 (0.178 ...	-0.11 (-0.38 ...	291.89

			0.291)	0.37)	
FGOALS-f3-H HighResMIP (1)	good	good	0.302 (0.200 ... 0.374)	0.062 (-0.39 ... 0.60)	261.41
MRI-AGCM3-2-H HighResMIP (1)	good	reasonable	0.328 (0.220 ... 0.387)	0.16 (-0.22 ... 0.69)	195.84
MRI-AGCM3-2-S HighResMIP (1)	good	good	0.261 (0.172 ... 0.317)	0.0013 (-0.45 ... 0.28)	178.19
CMIP6					
ACCESS-CM2 CMIP6 (1)	reasonable	bad	0.334 (0.197 ... 0.432)	-0.22 (-0.52 ... 0.17)	63.75
BCC-CSM2-MR CMIP6 (1)	reasonable	good	0.500 (0.356 ... 0.580)	0.18 (-0.37 ... 0.87)	280.34
CanESM5 CMIP6 (1)	bad	bad	0.430 (0.296 ... 0.497)	0.19 (-0.23 ... 0.80)	80.39
FGOALS-g3 CMIP6 (1)	reasonable	reasonable	0.267 (0.177 ... 0.321)	0.13 (-0.56 ... 0.50)	169.46
GFDL-ESM4 CMIP6 (1)	reasonable	reasonable	0.338 (0.254 ... 0.404)	0.13 (-0.69 ... 0.51)	172.77
IPSL-CM6A-LR CMIP6 (1)	good	reasonable	0.417 (0.296 ... 0.487)	0.14 (-0.26 ... 0.52)	124.55
MIROC6 CMIP6 (1)	reasonable	reasonable	0.221 (0.120 ... 0.292)	0.31 (-0.024 ... 1.1)	108.29
MRI-ESM2-0 CMIP6 (1)	reasonable	reasonable	0.276 (0.180 ... 0.335)	-0.13 (-0.72 ... 0.55)	76.40
NorESM2-LM CMIP6 (1)	reasonable	reasonable	0.173 (0.126 ... 0.205)	-0.0047 (-0.56 ... 0.33)	79.65

5 Multi-method multi-model attribution

This section shows Probability Ratios and change in intensity ΔI for models and also includes the values calculated from the fits with observations (see Table 2).

***Table 2**: Probability ratio and change in intensity of an event such as the Rx1day event under study in the models that pass model evaluation, (a) from pre industrial climate to the present and (b) from present to a future warmer word at 2C above pre-industrial levels.*

	(a) (a) -1.3C vs present		**(b) Present vs +0.7C**	
Model / Observations	**Probability ratio PR []**	**Change in intensity ΔI [%]**	**Probability ratio PR [-]**	**Change in intensity ΔI [%]**
IMD (1979-2024)	6.8 (0.11 ... 1.6e+6)	31 (-26 ... 1.7e+2)		
CPC	3.2 (0.38 ... 1.8e+2)	28 (-16 ... 99)		
IMD (1901-2024)	0.58 (0.067 ... 7.8)	-7.4 (-25 ... 16)		

MIROC5_rcp85_r1i1p1_RegCM4-7 CORDEX (1)	0.78 (0.26 ... 2.9)	-7.8 (-35 ... 36)	1.2 (0.96 ... 1.9)	6.9 (-1.3 ... 15)
MPI-ESM-LR_rcp85_r1i1p1_ETH-COSMO-crCLIM-v1-1 CORDEX (1)	2.0 (0.65 ... 7.4)	14 (-7.9 ... 39)	1.2 (0.81 ... 1.8)	3.0 (-3.8 ... 9.9)
MPI-ESM-MR_rcp85_r1i1p1_RegCM4-7 CORDEX (1)	1.3 (0.41 ... 6.3)	8.0 (-26 ... 55)	1.1 (0.80 ... 1.7)	3.8 (-8.5 ... 16)
NorESM1-M_rcp85_r1i1p1_ETH-COSMO-crCLIM-v1-1 CORDEX (1)	1.7 (0.20 ... 46)	7.8 (-24 ... 43)	0.89 (0.38 ... 1.7)	-1.7 (-11 ... 7.7)
FGOALS-f3-L HighResMIP (1)	1.6 (0.36 ... 18)	8.2 (-20 ... 40)	1.3 (0.63 ... 4.0)	4.7 (-12 ... 18)
FGOALS-f3-H HighResMIP (1)	0.72 (0.098 ... ∞)	-3.4 (-31 ... 36)	0.92 (0.16 ... 7.3)	-0.84 (-19 ... 15)
MRI-AGCM3-2-H HighResMIP (1)	0.77 (0.34 ... 3.2)	-6.7 (-27 ... 25)	0.79 (0.52 ... 1.6)	-6.8 (-21 ... 9.4)
MRI-AGCM3-2-S HighResMIP (1)	0.79 (0.15 ... 2.6e+2)	-2.9 (-25 ... 24)	0.87 (0.30 ... 3.1)	-1.6 (-16 ... 9.5)
IPSL-CM6A-ATM-HR HighResMIP (1)	1.9 (0.11 ... 93)	14 (-44 ... 1.2e+2)	1.4 (0.20 ... 5.9)	6.7 (-37 ... 35)
BCC-CSM2-MR CMIP6 (1)	0.47 (0.16 ... 2.8)	-16 (-37 ... 22)	1.2 (0.77 ... 1.9)	3.7 (-6.1 ... 12)
FGOALS-g3 CMIP6 (1)	1.9 (0.60 ... 5.4)	9.4 (-6.4 ... 26)	1.2 (0.83 ... 1.6)	2.5 (-2.5 ... 6.9)
GFDL-ESM4 CMIP6 (1)	6.7 (1.1 ... 1.7e+2)	36 (1.5 ... 74)	1.7 (1.2 ... 3.0)	9.4 (2.5 ... 16)
IPSL-CM6A-LR CMIP6 (1)	7.5 (2.6 ... 1.0e+2)	49 (24 ... 82)	1.6 (1.2 ... 2.4)	10 (4.1 ... 16)
MIROC6 CMIP6 (1)	1.3 (0.56 ... 4.5)	5.8 (-11 ... 30)	1.2 (0.92 ... 1.7)	3.3 (-1.6 ... 8.3)
MRI-ESM2-0 CMIP6 (1)	1.0 (0.35 ... 3.3)	-0.040 (-17 ... 18)	1.3 (0.94 ... 2.0)	4.5 (-0.90 ... 9.3)
NorESM2-LM CMIP6 (1)	12 (1.3 ... ∞)	16 (1.7 ... 30)	1.2 (0.71 ... 2.3)	1.7 (-2.2 ... 5.8)

6 Hazard synthesis

For the event definition described in Section 1.1 - RX1day over the monsoon season (June to September) in northern Kerala - we evaluate the influence of anthropogenic climate change by calculating the probability ratio as well as the change in intensity using observations and climate models. Models which do not pass the evaluation described in Section 4 are excluded from the analysis. The aim is to synthesise results from models that pass the evaluation along with the observations-based products, to give an overarching attribution statement. Figure 5 shows the changes in probability and intensity for the observations (blue) and models (red). Before combining them into a synthesised assessment, first, a representation error is added (in quadrature) to the observations, to account for the differences between observations-based datasets that cannot be explained by natural variability. If present, this is shown in these figures as white boxes around the light blue bars. The dark blue bar shows the average over the observation-based products. Next, a term to account for intermodel spread is added (in quadrature) to the natural variability of the models. This is shown in the figures as white boxes around the light red bars. The dark red bar shows the model average, consisting of a weighted mean using the (uncorrelated) uncertainties due to natural variability plus the

term representing intermodel spread (i.e., the inverse square of the white bars). Observation-based products and models are then combined into a single result in two ways. Firstly, we neglect common model uncertainties beyond the intermodel spread that is depicted by the model average, and compute the weighted average of models (dark red bar) and observations (dark blue bar): this is indicated by the magenta bar. Because, due to common model uncertainties, model uncertainty can be larger than the intermodel spread, secondly, we also show the more conservative estimate of an unweighted, direct average of observations (dark red bar) and models (dark blue bar) contributing 50% each, indicated by the white box around the magenta bar in the synthesis figures.

Satellite-era observations (45 years of records, beginning in the year 1979) and the majority of the models (9 out of 16 models that passed evaluation) show a tendency towards stronger and more frequent RX1day events like the one in July 2024;the remaining models (including the two HighResMIP models that ranked as 'good') lean towards decreases in the likelihood and intensity of extreme rainfall (Figure 5). The observed and modelled results are well within the uncertainty bounds of each other and thus do not show a systematic discrepancy; therefore, we report the synthesised weighted averages of the probability ratios and intensity changes as the overarching results.

In the observations, the best estimates for the change in intensity and likelihood of an event such as the 2024 event are sensitive to the length of the time series chosen. Considering only the last 45 years of records, the observations (indicated by the dark blue bars in Figure 5) suggest a strong increase in intensity and likelihood with 29.4% increase (95% confidence interval: 21.4 % decrease to 134% increase) and PR of 4.72 (0.17 to 17834). The full IMD time series (1901-2024) shows a slight decreasing trend, and when this is used instead of the shorter time series the overall signal is weaker, with intensity change of 8.8% increase (37.1% decrease to 90.2% increase) and a PR of 1.37 (0.05 - 81.2), as shown by the dark blue bars in Figure S4. Due to the large uncertainties around the observations and the relatively strong model consensus, the choice of whether to include only the satellite era has very little effect on the overarching synthesised conclusions from the study,which are reported below using the shorter time series.

After combining the results from the observations with findings from the 16 models that passed model validation, we find that a 50-year rainfall event in the current climate has been made 10.8% more intense (uncertainty: 3.3% decrease to 27.1% increase) due to the 1.3°C warming since the pre-industrial era. This is consistent with the Clausius-Clapeyron relationship that states that the atmosphere's moisture holding capacity increases by 7% for every one degree of warming. This is found to continue to hold after a further 0.7 °C of warming - the synthesised results from the models show a significant increase in the intensity of RX1day by 4.2% (uncertainty: 2.1% increase - 6.2% increase) (Figure 6), also in line with Clausius-Clapeyron scaling. The overall best estimate for the probability ratios between the pre-industrial past and now is 1.4 (uncertainty: 0.6 - 3.6) and from now to a future 0.7°C warmer climate is 1.27 (uncertainty: 1.14 to 1.44), suggesting that climate change has made an event such the 2024 JJAS RX1day more likely and will make similar events even more frequent under future warming.

We note that the HighResMIP models have only been used to attribute the effect of climate change since the preindustrial era on one-day rainfall maxima, and not to project the changes forward in time. This is because, at the time of writing, future GMSTs were not available to the authors for use as covariates in the statistical model fitting. Given that the HighResMIP models (FGOALS, MRI-AGCM3 and IPSL-CM6A-ATM-HR) simulated decreases or among the smallest increases, this risks introducing a bias into the synthesised future changes. The synthesis was repeated with the HighResMIP trends projected under a further 0.7°C of warming and was found to produce qualitatively similar conclusions (Figure S5).

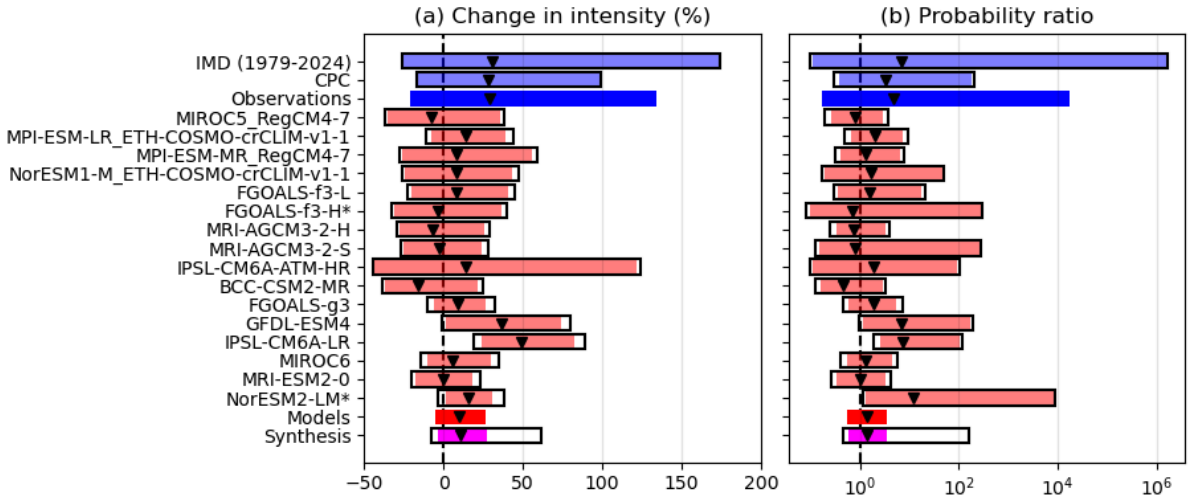

Figure 5: *Synthesis of (left) probability ratios and (right) relative intensity changes when comparing the return period and magnitudes of JJAS rx1day in the study region between the current climate and a 1.3C cooler climate. See text for further details.*

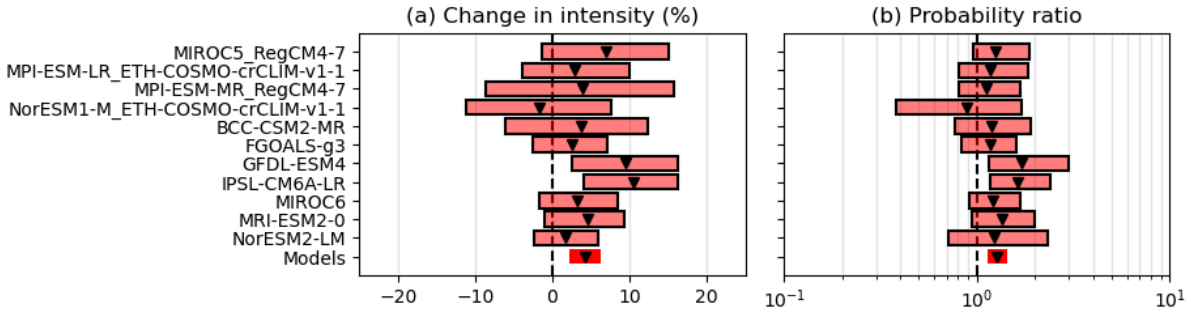

Figure 6: *As Figure 5, but synthesising changes in JJAS rx1day between the current climate and a 0.7C warmer climate (that is, a climate that is 2C warmer than preindustrial). See text for further details.*

7 Vulnerability and exposure

Kerala, located on the southwestern coast of India, features a diverse geography characterised by a coastal plain along the Lakshadweep Sea, fringed by the mountainous Western Ghats to the east. The district of Wayanad, situated on the southern tip of the Deccan Plateau, is characterised by dense forests, steep slopes, and deep valleys, and it is considered as one of the biodiversity hotspots of the Western Ghats. Wayanad supports a wide range of agricultural activities, including crops such as tea, banana, paddy, coffee, pepper, and various spices (Government of Kerala, 2016). With the smallest share of the state population (2.4%), the district is home to just over 800,000 residents (State Planning Board, 2017).

On July 30th, a total of about 80,000 square metres of land is estimated to have slipped, with debris flowing along the Chaliyar river, and one of its major tributaries, Iruvanjippuzha, for approximately 30 and 8 kilometres, respectively (The Hindu, 2024; The Economic Times, 2024), hitting the villages

of Chooralmala, Mundakai, Noolpuzha, Attamala, Meppadi, and Kunhome the hardest (Caritas, 2024; HAI, 2024). At the time of writing, 231 fatalities are confirmed by the state government (Sharif, 2024) and more than 400 fatalities reported by media (Singh, 2024) - a figure which is roughly equal to the cumulative death toll of the entire 2018 monsoon in Kerala (440 casualties); the state's most extreme monsoon season since 1924 (Hao et al., 2024). Among these victims, tea estate workers, often working as informal labourers (HAI, 2024), are reported to be disproportionately impacted (Lekhi & Maqbool, 2024). The landslides have severely disrupted the lives and devastated the livelihoods of residents across Wayanad, with the state government's initial estimates of property damage exceeding Rs 1,200 crore (US$140 million) (The Week, 2024).

Between 2015-2022, approximately 59% of India's 3,782 landslides occurred in Kerala (India Today, 2024; Ramasamy et al., 2020). Among Kerala's districts, Wayanad is one of the most susceptible to the hazard (Sharma, Sharia & Ramana, 2024; Ajmal & Saud, 2022; Hao et al., 2022). In 2018, 2019, and 2020, Kerala, including Wayanad, experienced significant losses and damages from landslides (Jain et al., 2020; Wadhawan et al., 2020). As demonstrated in figure 7, the highly susceptible zones overlap with forest and agriculture lands, including for Wayanad district, and the built up areas are located adjacent to these risk zones.

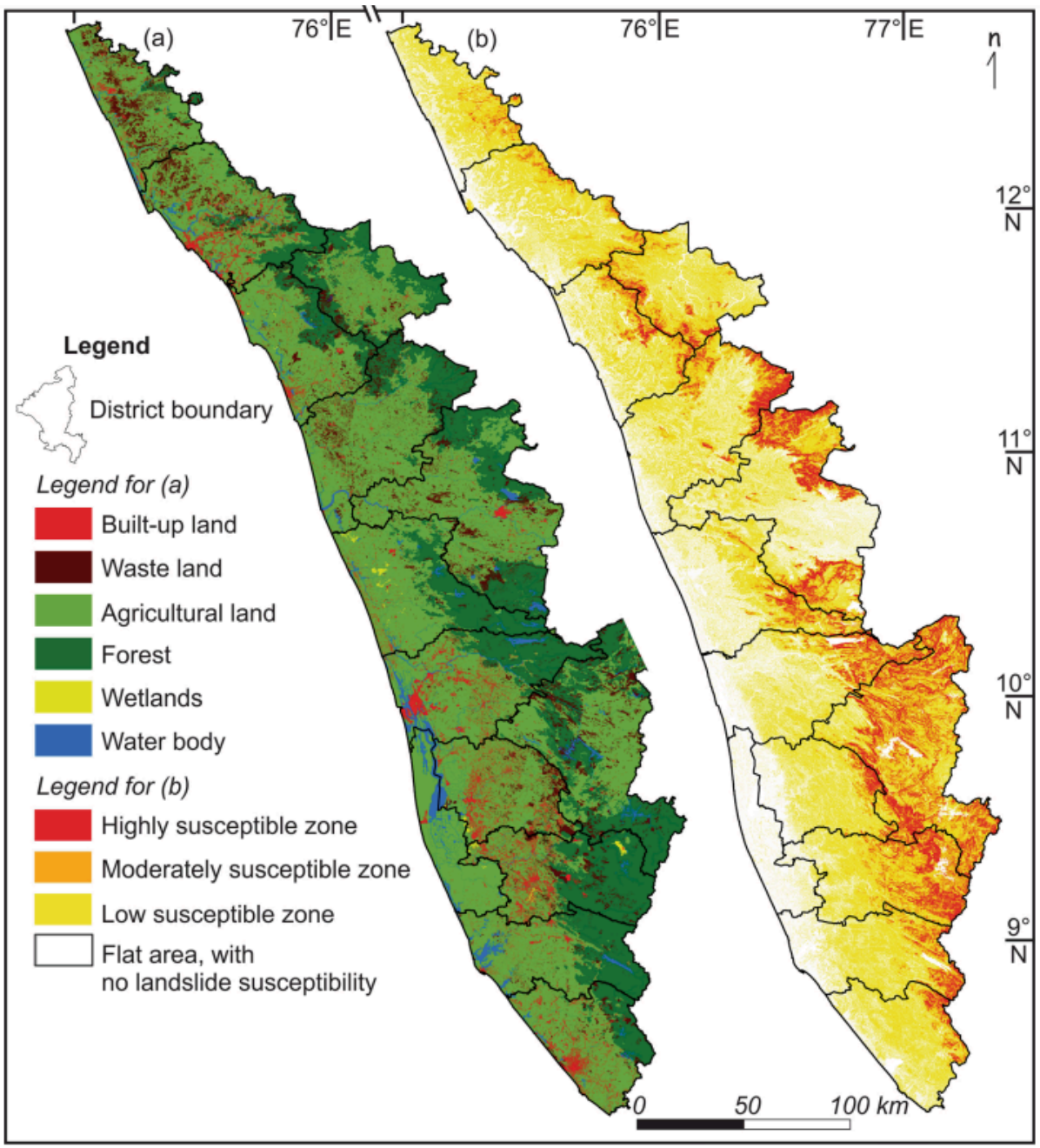

Figure 7. *Maps of (a) land-use, and (b) landslide susceptibility in Kerala. Source: Hao et al. (2022).*

Landslide risk is influenced by a range of factors, including slope angles, soil and rock characteristics, vegetation, drainage, deforestation, construction, and infrastructure development (Geological Survey of India, n.d.; Jones et al., 2021; Ajin et al., 2016), with heavy rainfall constituting the most common trigger (Ajmal & Saud, 2022). In this vulnerability and exposure analysis, we discuss land-use management and landslide risks in the region, to offer insights into the main drivers of risk which can also help explain the impacts associated with the 2024 landslides.

7.1 Land use land cover changes

For a hazard to cause losses and damages, (vulnerable) people, systems, and assets must be exposed to it. As such, land-use zoning regulations play a central role in mitigating landslide risk. The National Landslide Susceptibility Mapping (NLSM) programme in India, initiated in 2014 and led by the Geological Survey of India (GSI), offers a critical tool for state governments to prioritise resources and frame zoning regulations based on detailed landslide inventories (GSI, n.d.; Bhukosh, n.d.). Globally, land use and land cover (LULC) changes are also considered an important conditioning factor in rainfall-triggered landslides, with deforestation, road construction and building construction reducing slope stability while vegetation improves slope stability (Quevedo et al., 2023).

In Kerala and Wayanad, the evidence on the link between LULC and landslide events remains mixed. For 90% of the landslides which occurred in Kerala between 2010 and 2018, Hao et al. (2022) suggest that no "noticeable" LULC changes took place over the two preceding years. However, while a substantial portion of landslides in the district occurred in densely vegetated areas (58%), a significant number (25%) also originated in forest plantations and built-up areas; suggesting that land-use changes may indeed have played a role in these disasters. For example, in the 2018 Wayanad landslides, Vinayan & Gurugnanam (2020) pinpoint infrastructural development and stone quarrying as the causative factors. In the following year, unsustainable rubber cultivation practices on the steep slopes (up to 30 degrees) have been pegged as a major culprit for the landslides, including operating heavy earth movers to dig large rain pits, which, when waterlogged by the heavy monsoon, acted as a trigger (Sarun et al., 2021). Poor water drainage management and residential developments are also found to have constituted causative factors (Wadhawan et al., 2020).

Deforestation is the most pronounced land-use change in the district. Between 1950 and 2018, Wayanad lost 62% of its green cover, with tea plantation areas increasing by approximately 1800% (Saha et al., 2022), resulting in reduced forest cover to stabilise the hills. As demonstrated in figure 8, these changes had significantly altered the face of the district already in 2012, after which plantations continued to expand from 913 to 1215 km2 while forests shrunk from 888 to 672 km2.

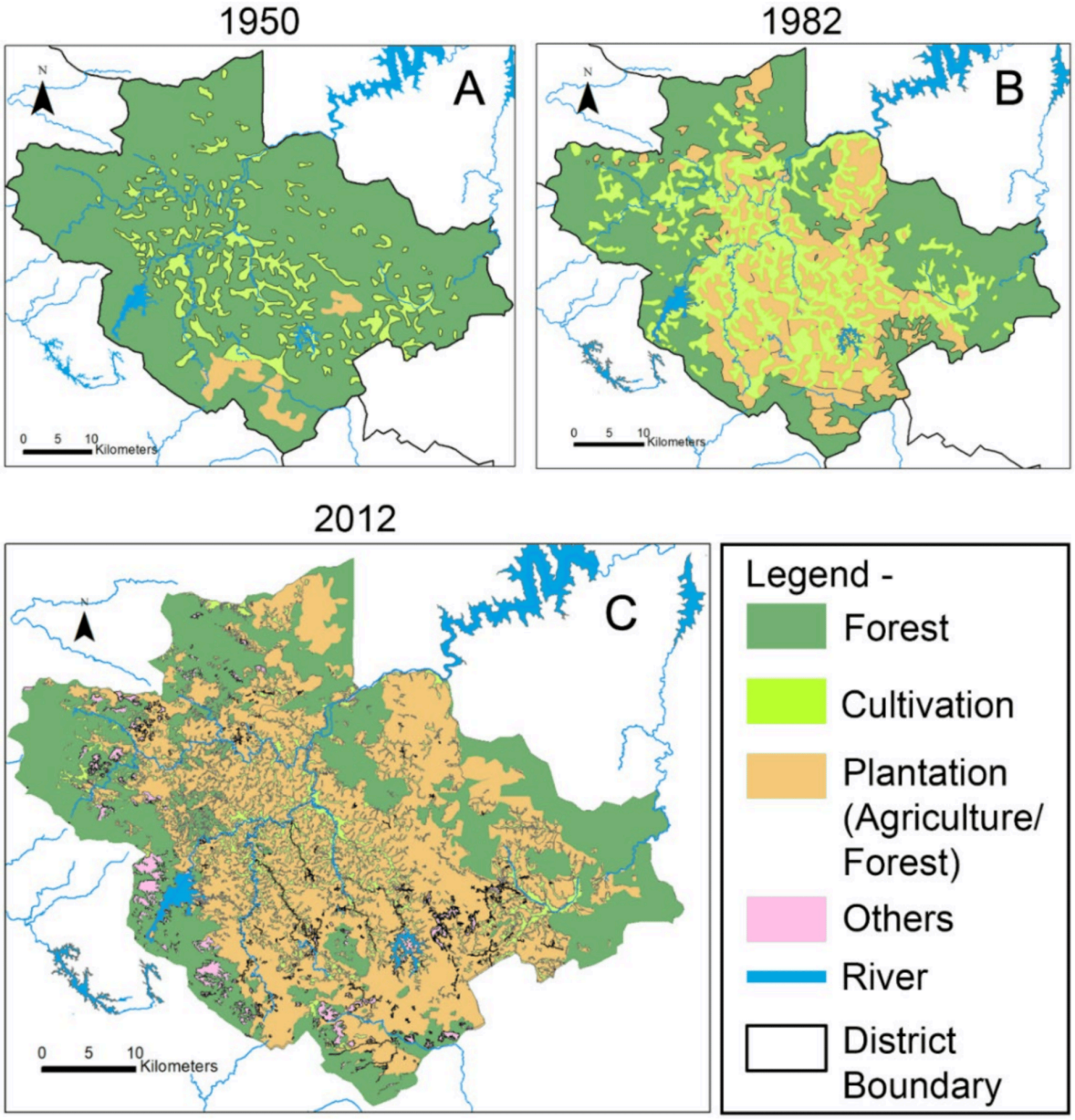

Figure 8. *Land-use changes in Wayanad district between 1950-2012; land use land cover in (A) 1950; (B) 1982; and (C) 2012. Source: Saha et al. (2022).*

There has been quarrying for building stones in the Wayanad area in recent years that raise concerns amongst scientists as the activity could impact slope stability. For example, one study in Banasuramala, Wayanad District found that existing curvilinear cracks were stable under dry conditions, but become critical under wet and saturated conditions increasing the risk of land disturbances during the monsoon season (Sajinkumar et al., 2014). There are conflicting claims about the existence of illegal quarrying and quarry permits following the 2018 flood and disaster in this region (The Wire, 2024; Perinchery, 2024). For example, one study published in 2021 identified 131 granite quarries in Wayanad district, of which 24 were actively operational (Vimod & Praveen, 2021). This included 15 active quarries near previous landslide locations, leading the authors to recommend

that continued quarrying activities be limited to localities with no threat of landslides (Vimod & Praveen, 2021).

7.2 Early warning early action

Effective early warnings which lead to early actions are critical in mitigating landslide risk. To this end, it is imperative that warnings reach those at risk, and that people understand and use the information to act in ways which help protect health, livelihoods, assets, infrastructure, and the environment (Golding, 2022). While India, Kerala, and Wayanad face recurring landslides, it is important to note that landslides are notoriously difficult to predict and thus complicated to monitor and warn for. The implementation of landslide early warning systems (LEWS) in India is still in the developmental stages. In July 2024, the Geological Survey of India (GSI) launched the National Landslide Forecasting Centre, which currently only provides daily forecasts for select regions, namely West Bengal and Tamil Nadu.

In response to recent landslide disasters, Kerala has intensified its focus on improving LEWS (Abraham et al., 2019). Since 2020, GSI, Kerala University, and Kerala Development & Innovation Strategic Council (L-DISC) have joined forces to develop a pilot LEWS for select locations across the state (Kerala State Disaster Management Authority, n.d.). Local institutions, such as Amrita Vishwa Vidyapeetham, have also developed innovative solutions, including a real-time wireless sensor network for landslide detection. This system, deployed in Idukki district, successfully predicted a landslide in 2009, demonstrating the potential of slope-specific LEWS (Amrita, n.d.; Krishnamurthy, 2024). However, the cost of implementing such systems on a large scale remains prohibitive, especially given the high number of active landslides in the country (Krishnamurthy, 2024). As a result, researchers advocate for regional rather than site-specific early warning systems, except in areas with high population density and landslide susceptibility. Moreover, challenges remain in fully operationalizing some of these systems due to gaps in critical data among the complex landscape of rain and soil parameters essential to developing a LEWS (see figure 9), such as soil thickness and real-time weather information from automated stations (Krishnamurthy, 2024). As set forth in GSI's Vision 2030 (GSI, n.d.), the national LEWS will expand to ensure coverage of risk zones across Kerala, along with India's other 15 landslide-prone states and two Union Territories.

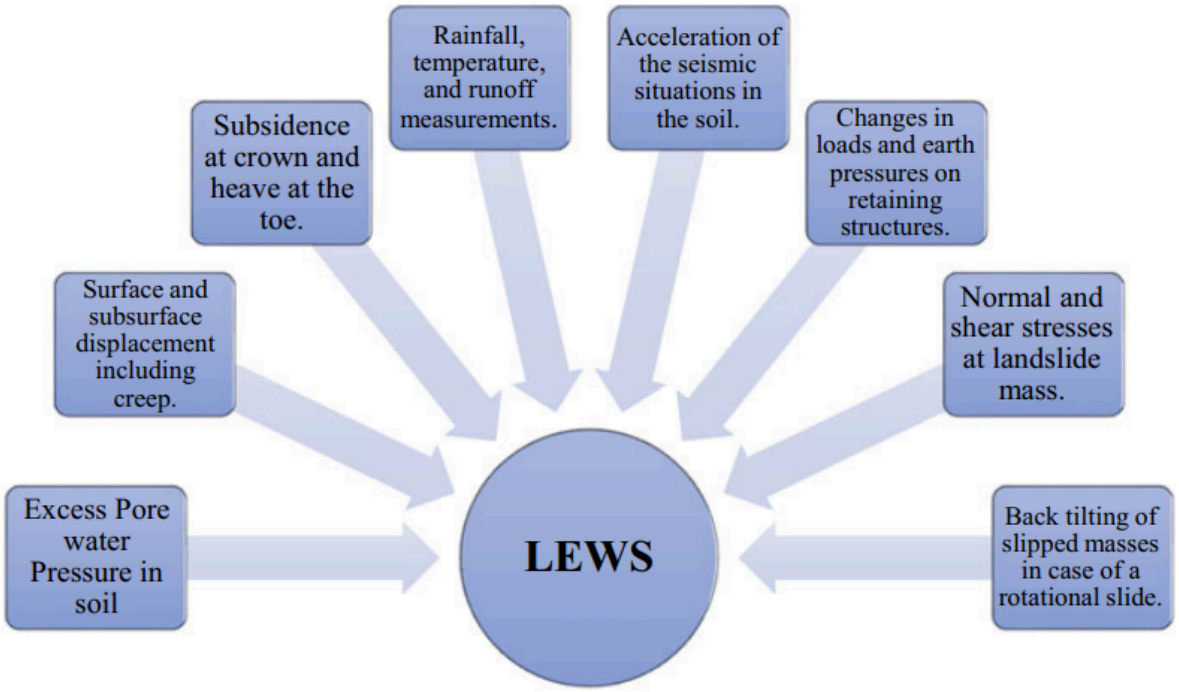

Figure 9. *A variety of soil parameters which can be employed to develop a landslide early warning system. Source: Menon & Kolathayar (2022).*

On Sunday July 28th, a day and a half prior to the onset of the first landslide, the India Meteorological Department (IMD) issued a press release (IMD, 2024a) and bulletin (IMD, 2024b) forecasting "heavy" (≥7 cm) to "very heavy" (≥ 12 cm) "rainfall very likely at isolated places" across Kerala on July 29th and 30th. The former detailed the risk of localised land and mud slides, slips, and sinks, along with suggested actions such as avoiding "staying in vulnerable structure". The same forecast was presented in the press release (IMD, 2024c) and bulletin of the 29th (IMD, 2024d), published at 1:30pm and 4:30pm IST, respectively. Approximately 12 hours later, during the early hours of Tuesday July 30th, the first landslide struck (Mishra, 2024; HAI, 2024). At 1:10pm on Tuesday the 30th, IMD (2024e) issued a press release warning of "isolated extremely heavy rainfall likely over Kerala [...] on 30th".

On the 29th, residents of Attamala and Mundakkai, two of the hardest-hit villages, were evacuated to shelters due to the heavy rainfall (Mano, 2024). However, there are also reports of people remaining unaware of the dangers or being reluctant to leave their home (Mishra, 2024). The degree to which the warning information reached, was understood by, and provided adequate instructions to all individuals and households in the at-risk areas remains unclear, and will be essential to research and evaluate in the recovery phase to learn from the event.

The Wayanad disaster underscores the need for a more robust and localised early warning system that can provide accurate, timely, and actionable alerts to vulnerable communities, which are understandable to all and contain precise advice on actions to take after receiving a warning. This requires not only technological enhancements but also improved coordination between government

agencies and local communities to ensure that early warnings translate into effective early actions, ultimately saving lives.

7.3 Emergency response

The central and decentralised state governments' responses are substantial, including, for examples, the relocation of residents, rebuilding of infrastructure, transportation of essential medical aid and rescue equipment to affected areas, and announcing financial support to those who have lost family members in the disaster (HAI, 2024). Among the numerous non-governmental and community-based organisations, for example, the Indian Red Cross Society (IRCS) has mobilised relief supplies and volunteers available in Kerala and neighbouring states to supplement the rescue and relief measures initiated by the local Red Cross branch and administration for the survivors (IRCS, 2024). In addition to the relief supplies and support by the Kerala State branch, the national headquarters has released kitchen sets, tents and tarpaulins to meet the urgent needs of the displaced and others affected. Caritas India (2024), another humanitarian actor responding to the disaster, is working to ensure that households have their basic needs met, restoring livelihoods, rebuilding housing, and strengthening community resilience to future shocks.

Despite the rapid deployment of the numerous forces, rescue operations faced severe obstacles due to the region's difficult terrain and the scale of the disaster (Times of India, 2024). The collapse of the main bridge to one of the hardest-hit areas significantly hampered access, necessitating the construction of a temporary 58-metre Bailey bridge by the Army to reach communities in need of humanitarian assistance (Lekhi & Maqbool, 2024; HAI, 2024). Additionally, the Chaliyar River's force swept away many victims, complicating search and rescue efforts, with bodies being recovered up to 30 kilometres from the landslide site (Lekhi & Maqbool, 2024). The inaccessibility of certain areas along the river further delayed rescue operations (Onmanorama, 2024).

V&E conclusions

Wayanad is a highly landslide-prone region, with one of the highest risk in the state of Kerala. While early warning of extreme rainfall and the potential for landslides was shared by the IMD, the information was not tailored or specific to the places that would eventually see the landslides. These state-level warnings are often ineffective because they do not specify which particular slopes are most at risk and cover thousands of people, making it difficult to encourage early action. However, slope-specific landslide early warning systems are extremely costly and difficult to implement, but would provide the best opportunity for effective early action. Given this challenge, it is important to focus on reducing landslide exposure overall.

Land use and land cover changes can either increase or decrease the susceptibility of slopes to landslide risks, but in Wayanad the evidence is mixed in which some studies point to a linkage and others do not. A significant shift in recent years has been the 62% reduction in forest cover, which may have played a role in reducing soil stability on those slopes. In addition, quarrying activities have been linked to increased slope instability, especially during the monsoon season, and studies show their continuation despite efforts to reduce illegal quarrying. However, there are measures that can be taken to minimise the effects of quarrying such as using controlled blasting, pausing mining during

the monsoon season, and constructing interconnected surface drains, amongst others (Sajinkumar et al., 2014).

The increase in climate change-driven rainfall found in this study is likely to increase the number of landslides that could be triggered in the future. However, there are measures that can reduce the "conditioning factors" that increase landslide risk such as by planting suitable vegetation on slopes and protecting forest reserves. In addition, draining solutions as well as retaining walls can be constructed to reduce landslide risks, and awareness can be raised amongst local people to avoid construction near or along drainage paths or at the top or base of landslide prone areas (Jain et al., 2021).

Data availability

All of the time series used in this study are available via the Climate Explorer.

References

All references are given as hyperlinks in the text.

Supplement

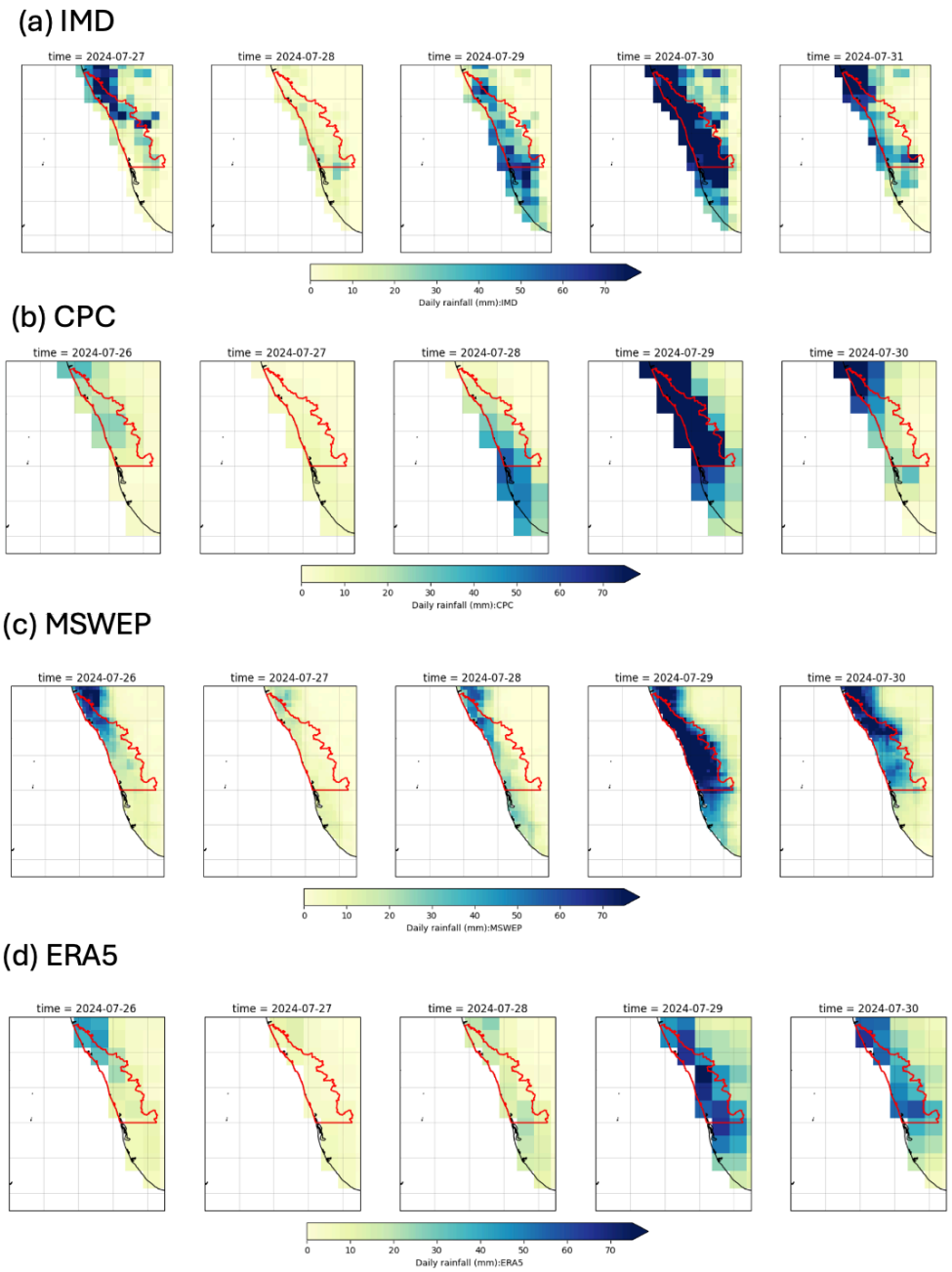

Figure S1: *(a) Daily rainfall during 27-31 July, 2024 in IMD. (b) Daily rainfall during 26-30 July, 2024 in (b)CPC, (c) MSWEP and (d) ERA5 datasets.*

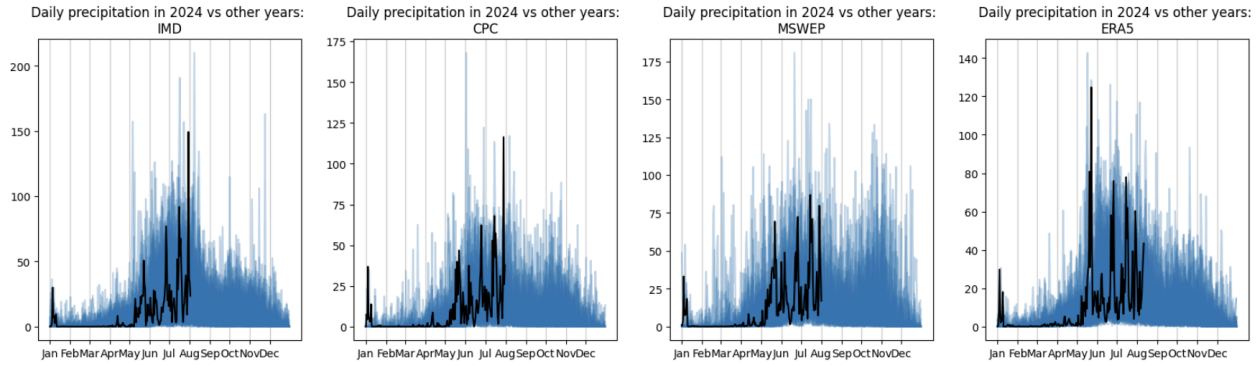

***Figure S2**: Daily rainfall in the year 2024 vs all other available years in (a) IMD (b) CPC © MSWEP and (d) ERA5 datasets*

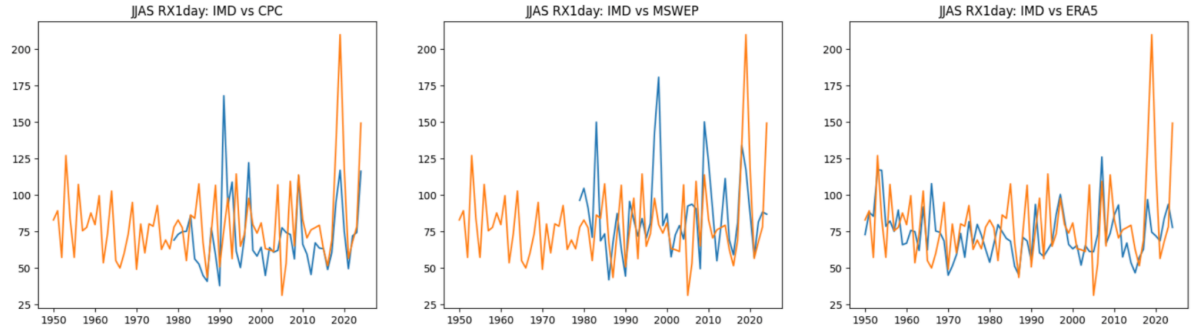

***Figure S3:** Annual time series of JJAS RX1day, area-averaged over the study region for the three gridded datasets against IMD: (a) CPC (b) MSWEP (c) ERA5.*

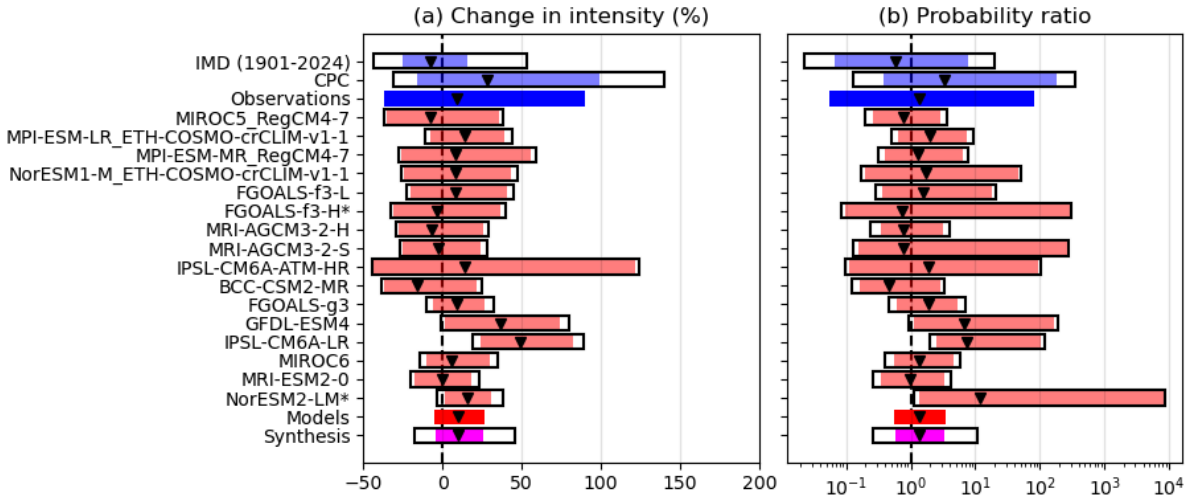

***Figure S4:** As Figure 5, but using the full IMD time series (1901-2024), rather than just the satellite era. The overall synthesised results (purple bars) are very similar to those presented in Section 6, with the change in intensity estimated to be 9.6% (95% confidence interval: -4.4% to 25.7%) and the probability ratio estimated to be 1.3 (0.6 to 3.4).*

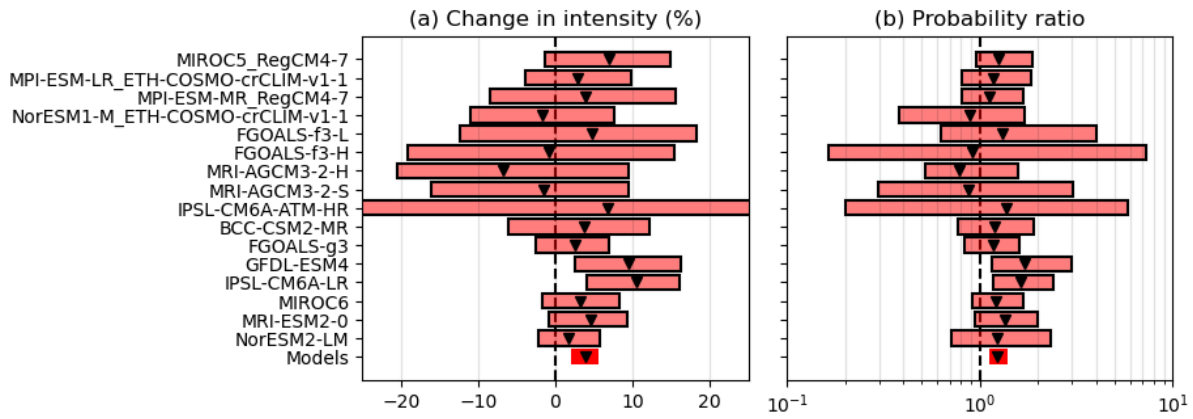

Figure S5: *As Figure 6, but including the projected changes for the HighResMIP models. See text for further details. The x-axis of (a) is truncated to allow direct comparison with Figure 6: the 95% confidence interval for IPSL-CM6A-ATM-HR is (-37, 35). The synthesised model results (dark red bar in each plot) are very similar to those presented in Section 6, with the change in intensity estimated to be 4.0% (95% confidence interval: 2.1% to 5.7%) and the probability ratio estimated to be 1.24 (1.11 to 1.40).*